# Design of a three-dimensional gap-coupled suspended substrate stripline bandpass filter

Y.-C. Chiang
C.-K.C. Tzuang
S. Su

*Indexing term: Filters and filtering*

**Abstract:** A three-dimensional gap-coupled suspended substrate stripline (SSS) bandpass filter, based on the modified configuration of the classic end-coupled filter, is presented. It consists of printed half-wavelength resonators placed on the same and/or the opposite sides of the suspended substrate. These resonators orient themselves in arbitrary directions. Such an arrangment makes the new filter highly flexible to interface with other microwave subcircuit modules. The filter is constructed in a bent channelised housing that suppresses any possibility of exciting higher-order modes, except the dominant quasi-TEM mode of propagation. Consequently, the channelised filter is free from any coupling between itself and other microwave circuit components within the system. Two look-up tables, derived from a variational three-dimensional quasi-TEM spectral-domain analysis of the discontinuity problems associated with the adjacent gap-coupled resonators, are incorporated into the computer-aided design of the new filter. The de-embedded discontinuity parameters are validated by comparing them with those obtained by experiment and full-wave approaches for the microstrip open-end and the SSS end-coupled problems, respectively. The measured results for the experimental 21–22 GHz bandpass filter agree very well with the theoretic predictions considering the conductor losses ($5.57 \times 10^{-3}$ dB/mm) of the SSS. It has less than 1.4 dB insertion loss and greater than 10 dB return loss in the passband.

## 1 Introduction

The suspended substrate stripline (SSS) has been widely adopted in a variety of microwave and millimetre-wave filter designs [1–11]. When compared with other planar or quasiplanar transmission lines, the SSS has the following merits: high unloaded Q, low-loss [1–6], insensitivity to temperature variation, as most of the electromagnetic energy of the SSS is essentially distributed in the air [1, 2], wider bandwidth [1–3, 5–8, 11], and broadband low-loss transition to a rectangular waveguide [7–10]. Given a required impedance level, e.g. 50 Ω, the SSS is wider than most stripline-based planar or quasiplanar transmission lines integrated on the same printed-circuit substrate. This makes the SSS filters highly reproducible at low cost, using conventional photolithography technologies.

Among various SSS filters reported [1–11], Rhodes and Dean developed a design approach incorporating the mixed lumped and distributed circuits [1–3]. Using such an approach as a basis, they reported several broadband lowpass, highpass and bandpass filters operated at frequencies ranging from 0.5 to 40 GHz. By series or parallel connecting two or more lowpass and highpass filters, various broadband SSS filters, such as diplexers and multiplexers, were also reported.

The highpass filters designed by Rhodes and Dean [1–3] often mandate the use of strongly coupling elements for certain broadband applications. Therefore the broadside-coupled SSSs are applied to meet such needs. As the filter performance is highly dependent on these broadside SSS coupling elements, the precise determination of the dimensions of the coupling elements becomes one of the key issues for designing a high-performance broadband filter. Rhodes and Dean also employed the microwave circuit model proposed by Zysman and Johnson [12], who developed the equivalent circuit representation of the inhomogeneous parallel-coupled lines using quasi-TEM approximations, to analyse the symmetric broadside-coupled SSSs. The total fringing field effects of the sides and ends of the strips on the broadside-coupled SSSs, however, were approximated using the results obtained previously in Reference 3. By adopting the same technique, Mobbs and Rhodes [4] used the SSS broadside-coupled structures connecting with the high-impedance transmission lines to approximate the series LC circuit elements in a bandpass filter prototype. Based on such an approach, a 5–5.5 GHz bandpass filter, with more than 20 dB return loss and less

Paper 8915H (E12), first received 4th December 1991 and in revised form 22nd April 1992

The authors are with the Institute of Electrical Communication Engineering, Microelectronic and Information Science Research Centre, National Chiao Tung University, 1001 Ta Hsueh Road, Hsinchu, Taiwan, R.O.C.

The authors would like to thank C.-D. Chen and J.-T. Kuo for their great help in providing the theoretic values of the complex propagation constant and the cut-off frequency of the first higher-order mode of the suspended substrate stripline. Thanks are also due to Steve Cheng for his assistance in obtaining the experimental results. This work was supported by the National Science Council, R.O.C., in part under Grant NSC81-0404-E009-120 and in part under Contract CS80-0210-D001-21.

than 1 dB insertion loss in the passband, was reported [4]. Lösch and Malherbe extended the work of Zysman and Johnson by including the effect of the open-end fringing capacitances in the expressions of the effective dielectric constants for even the odd modes, respectively. Accordingly, they have designed and tested a 2–9 GHz psuedo-high-pass filter with a maximum 0.4 dB insertion loss [5].

The circuit models developed by Zysman and Johnson were unsuitable for application in distributed filter synthesis [6]. To remedy the problem, Levy theorised a new equivalent circuit model of the inhomogeneous coupled line section, which consisted of a pair of series-connected unit elements in series with two open-circuited stubs and two uncoupled transmission lines. By using such an approach, a 6–18 GHz pseudo-high-pass filter with insertion loss less than 1 dB was demonstrated [6].

On the other hand, the concept of admittance inverters was applied to design the parallel-coupled and end-coupled SSS bandpass filters [7–11] with operating frequencies up to millimetre-wave (30–300 GHz). Rubin and Hislop used two step impedance resonators, replacing the first and last parallel-coupled resonators in a 28–37 GHz parallel-coupled bandpass filter, to achieve 28% fractional bandwidth [7]. Ton *et al.* further adopted the synthesis technique developed by Rhodes [13], and designed an 18–30 GHz parallel-coupled SSS filter with 50% fractional bandwidth, using high-resolution photolithography printed circuit board technology [8]. The end-coupled filters are rather lengthy in comparison with other types of printed circuit filter, but are suitable for higher microwave frequencies where large size is sometimes advantageous. For instance, Nguyen and Chang reported the end-coupled SSS filter with passband at 32–35 GHz [9], and Dougherty reported a three-resonator end-coupled SSS filter operated at 45 GHz [10]. To avoid difficulty in increasing the bandwidth of the end-coupled filter, Tzuang *et al.* reported a broadside end-coupled SSS filter which easily achieved 30% fractional bandwidth in K-band [11].

In contrast to the conventional colinear realisations of the end-coupled [9, 10] or broadside end-coupled [11] SSS filters, a new three-dimensional implementation of the gap-coupled SSS bandpass filter is shown in Fig. 1. The half-wavelength resonators of this filter are located on the same and/or the opposite sides of the suspended substrate and can orient themselves in any arbitrary direction. Because the coupling between the adjacent resonators can be either end-coupled or broadside-coupled in arbitrary angles, the new filter configuration is named gap-coupled to reflect realistically its physical structure. The evolution from the conventional design to the new structure makes the filter much more complicated in shape. The new filter, however, has the following merits: It is highly flexible to interface itself with other microwave or millimetre-wave subcircuits in a communication system, because the resonators can change their orientation. Secondly, the new filter configuration is channelised in a controlled way, i.e. all the cutoff frequencies of the higher-order modes are far beyond the desired upper stopband frequency. Thus, only the quasi-TEM mode and higher-order evanescent modes are allowed to exist in the channelised filter. These evanescent modes quickly attenuate nearby any discontinuities associated with the filter. Thus, no cross-coupling between the channelised filter and any other microwave components can exist in system integration. Furthermore, the well-developed filter synthesis technique assuming a TEM mode of propagation can be applied here with confidence. This makes the filter characteristics highly predictable in both passband and stopband frequencies.

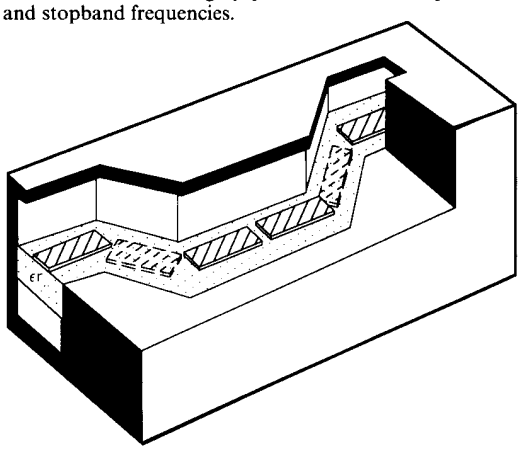

**Fig. 1** *Three-dimensional implementation of the channelised gap-coupled suspended substrate stripline bandpass filter*

The SSS resonators with solid lines are on the top surface of the suspended substrate; those with broken lines are on the bottom side of the substrate. The resonators can orient themselves in any arbitrary direction

The asymmetric gap-coupled discontinuities inherently present in the filter shown in Fig. 1, however, cannot possibly be determined by the above-mentioned equivalent circuit approaches [1–6]. Instead, a de-embedding procedure based on the three-dimensional quasi-TEM spectral-domain approach (SDA), which is the extended form of the two-dimensional SDA reported by Itoh [14], is incorporated in our computer-aided design (CAD) program and will be described in Section 2. To ensure the accuracy of the de-embedded discontinuity parameters, a new set of two-dimensional basis functions to describe the charge distribution on the assumed infinitely thin metal strip is used.

The validity of the de-embedded discontinuity parameters obtained by the three-dimensional quasi-TEM SDA is confirmed in Section 2.3 by comparing the theoretic results against the published data for the microstrip open-end and SSS end-coupled problems. This also demonstrates the fact that the static equivalent capacitances of discontinuities in many planar waveguides supporting quasi-TEM modes will result in data having very good agreement with measurements as reported by Naghed and Wolff [15].

Section 3 describes the filter design procedure as outlined by Matthaei *et al.* [16] for a 21–22 GHz three-resonator bandpass filter prototype, with its input and output ports located at the same reference plane. Such a filter has essentially zero compressed length. Section 4 confirms the accuracy of the design approach presented here by experimental evaluation of the prototype. The overall photolithography resolution tolerance for the fabricated filter is less than 0.02 mm. No tuning was necessary for the desired filter characteristics. The trial filter shows excellent agreement between the predicted filter performance and the measured data in both passband and stopband.

## 2 De-embedding of discontinuity parameters of gap-coupled resonators based on three-dimensional quasi-TEM SDA

Fig. 2*a* shows the top view and the longitudinal-section view of a hypothetical three-resonator gap-coupled

bandpass filter. The side walls of the channelised housing are reshaped to be rectangular with dimension $a \times b$. The lower and upper ground planes are kept the same. The three resonators are designated as $R_i$, $R_{i+1}$ and $R_{i+2}$ in Fig. 2a, respectively. Resonator $R_i$, drawn in broken lines, is located at $z = h_i$. Resonators $R_{i+1}$ and $R_{i+2}$, drawn in solid lines, are located at $z = h_1 + h_2$. Let $P_i$ and $P_{i+1}$ be located at the central end points of the adjacent gap-coupled resonators, respectively. The relative position between the adjacent gap-coupled resonators $R_i$ and $R_{i+1}$, for example, is described by the four gap discontinuity parameters $t_i$, $\psi_i$, $u_i$ and $v_i$. Parameter $t_i$ is the vertical distance between the adjacent resonators along the $z$ direction, and only two values can be chosen, either $t_i = 0$ or $t_i = h_2$. The former implies that the adjacent resonators are on the same side of the substrate, whereas the latter implies that they are on opposite sides. $\psi_i$ is the angle between the centrelines of the projection of the resonator $R_i$ and that of the resonator $R_{i+1}$ in the horizontal $x$–$y$ plane. The value of $u_i(v_i)$ is determined by subtracting the $x$-component ($y$-component) value of the projected point $P_i$ from that of point $P_{i+1}$. Therefore the values of $u_i$ and $v_i$ can be either positive or negative. The central point of the resonator $R_{i+1}$ projected in the $x$–$y$ plane is denoted as $(x_{i+1}, y_{i+1})$.

Fig. 2b shows the equivalent $\pi$-circuits of $R_i$, $R_{i+1}$ and $R_{i+2}$ in Fig. 2a, respectively. The susceptance parameters at reference planes 1 (2) and 1′(2′), i.e. $B_{si}(B_{si+1})$ and $B_{pi}(B_{pi+1})$, are critical to the first-time success of the filter design without any tuning. As the symmetry in the conventional colinear realisation of the end-coupled filter no longer exists in Fig. 2a, an accurate and reliable method to de-embed the discontinuity parameters must be developed.

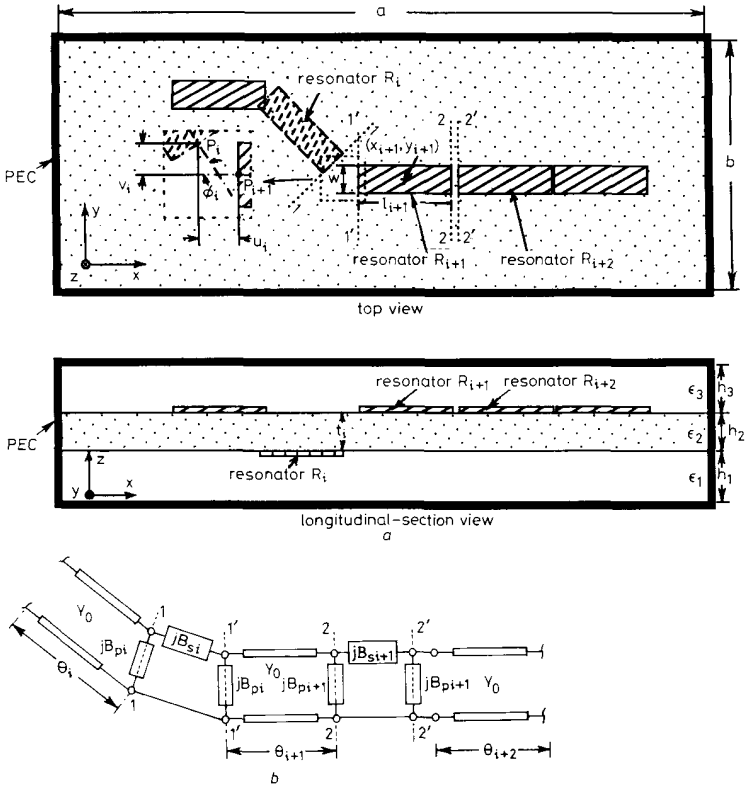


**Fig. 2** *Hypothetical three-resonator gap-coupled bandpass filter*

The side walls of the channelised housing are reshaped to be rectangular, with dimension $a \times b$. The lower and upper ground planes are kept the same
*a* Top view and longitudinal-section view of the filter: resonators located at $z = h_1$ and $z = h_1 + h_2$ are shown by broken and solid lines, respectively
*b* Equivalent $\pi$-circuit representation of $R_i$, $R_{i+1}$ and $R_{i+2}$ in *a*

Section 2.1 briefly describes how to obtain an accurate capacitance matrix by employing the three-dimensional quasi-TEM SDA. Followed by a conventional method for de-embedding the discontinuity parameters assuming quasi-TEM mode [11, 17], Section 2.2 explains how the susceptance parameters in the $\pi$-circuit of the gap-coupled discontinuities shown in Fig. 2 are obtained. The validity check of the de-embedding process described here is performed in Section 2.3. The results confirm the accuracy of our approach. Finally, Section 2.4 plots the discontinuity parameters necessary for carrying out the experimental filter design described in the following section.

### 2.1 *Three-dimensional quasi-TEM spectral-domain approach*

Under the quasi-TEM assumption, we only need to solve the laplace equation in an electrically shielded enclosure, subject to appropriate boundary conditions. Instead of solving such a problem directly in the space ($x$, $y$, $z$)

domain, we will work in the Fourier transform domain and introduce the two-dimensional Fourier transform of the potential function $\Phi(x, y, z)$

$$\tilde{\Phi}(m, n, z) = \int_0^a dx \int_0^b dy \Phi(x, y, z) \times \sin[(m\pi/a)x] \sin[(n\pi/b)y] \quad m = 1, 2, \ldots, \infty \quad n = 1, 2, \ldots, \infty \quad (1)$$

so that the partial differential equation (Laplace equation) becomes an ordinary differential equation through the previous transformation.

$$\left[\frac{d^2}{dZ^2} - (m\pi/a)^2 - (n\pi/b)^2\right]\tilde{\Phi}(m, n, z) = 0 \quad (2)$$

where $a$ and $b$ are the dimensions of the housing bounded by perfectly conducting side walls, as shown in Fig. 2*a*. By imposing the boundary conditions at $z = h_1$ and $z = h_1 + h_2$ in solving eqn. 2, one may obtain the following coupled algebraic equations:

$$\tilde{G}_{11}(m, n)\sum_{j=1}^{R}\tilde{\rho}_j(m, n) + \tilde{G}_{12}(m, n)\sum_{j=R+1}^{Nr}\tilde{\rho}_j(m, n) = \tilde{V}(1) + \tilde{v}(1) \quad (3a)$$

$$\tilde{G}_{21}(m, n)\sum_{j=1}^{R}\tilde{\rho}_j(m, n) + \tilde{G}_{22}(m, n)\sum_{j=R+1}^{Nr}\tilde{\rho}_j(m, n) = \tilde{V}(2) + \tilde{v}(2) \quad (3b)$$

where $\tilde{\rho}_j$ is the unknown charge distribution on the $j$th resonator; $R$ is the number of resonators located at $z = h_i$; $(N_r - R)$ is the number of resonators located at $z = h_1 + h_2$ and $\tilde{V}(1)$ and $\tilde{v}(2)$ are the Fourier transform of the given potentials on the resonators and equal to zero outside the resonators at $z = h_1$ and $z = h_1 + h_2$, respectively. Similarly, $\tilde{v}(1)$ and $\tilde{v}(2)$ are the Fourier transform of the potential distributions outside resonators and equal to zero on the resonators. $\tilde{G}_{11}$, $\tilde{G}_{12}$, $\tilde{G}_{21}$ and $\tilde{G}_{22}$ are Green's functions in the Fourier transform domain. To solve the unknown charge distribution $\tilde{\rho}_3$, the Galerkin method is applied [14]. The unknown charge distribution on a resonator can be expressed as

$$\tilde{\rho}_j(m, n) = \sum_{t=1}^{T_j} a_j^t \tilde{\xi}_j^t(m, n) \quad j = 1, 2, \ldots, N_r \quad (4)$$

where $T_j$ represents the number of basis functions used to expand the unknown charge distribution on the $j$th resonator, $a_j^t$ is the unknown coefficient to be determined and $\tilde{\xi}_j^t$ is the Fourier transform of an assumed space domain charge distribution $\xi_j^t(x, y)$, or the so-called basis functions. Substituting eqn. 4 into eqn. 3 and taking the inner products of the resulting equations with weighting functions $\tilde{\xi}_k^s$, for $k = 1, 2, \ldots, N_r$, and $s = 1, 2, \ldots, T_k$, then one may obtain the following $\sum_{j=1}^{Nr} T_j \times \sum_{j=1}^{Nr} T_j$ matrix equations for the unknown coefficient $a_j^t$, $j = 1, 2, \ldots, N_r$, and $t = 1, 2, \ldots, T_j$:

$$\sum_{m=1}^{M\to\infty}\sum_{n=1}^{N\to\infty}\tilde{\xi}_k^s(m, n)\left[\tilde{G}_{11}(m, n)\sum_{j=1}^{R}\sum_{t=1}^{T_j}a_j^t\tilde{\xi}_j^t(m, n) + \tilde{G}_{12}(m, n)\sum_{j=R+1}^{Nr}\sum_{t=1}^{T_j}a_j^t\tilde{\xi}_j^t(m, n)\right] = P_k^s(1) \quad (5a)$$

$$\sum_{m=1}^{M\to\infty}\sum_{n=1}^{N\to\infty}\tilde{\xi}_k^s(m, n)\left[\tilde{G}_{21}(m, n)\sum_{j=1}^{R}\sum_{t=1}^{T_j}a_j^t\tilde{\xi}_j^t(m, n) + \tilde{G}_{22}(m, n)\sum_{j=R+1}^{Nr}\sum_{t=1}^{T_j}a_j^t\tilde{\xi}_j^t(m, n)\right] = P_k^s(2) \quad (5b)$$

where

$$\tilde{P}_k^s(i) = \sum_{m=1}^{M\to\infty}\sum_{n=1}^{N\to\infty}\tilde{\xi}_k^s(m, n)[\tilde{V}(i) + \tilde{v}(i)] = \sum_{m=1}^{M\to\infty}\sum_{n=1}^{N\to\infty}\tilde{\xi}_k^s(m, n)\tilde{V}(i) = \frac{ab}{4}\int_0^a dx\int_0^b dy\xi_k^s(x, y)V(i) \quad i = 1, 2 \quad (6)$$

In the practical calculation, the spectral terms $M$ and $N$ are the finitely large numbers above for which the calculated results are almost the same. In the derivation of eqn. 6, we apply the Parseval relation. The second infinite summation in eqn. 6 vanishes, because the assumed charge distribution $\rho_j$ is zero outside the resonators, whereas the potential distribution $v_i$ is equal to zero on the resonators. As $V(i)$, $i = 1$ or 2, is the given potential on the resonators, $\tilde{P}_k^s(i)$ in eqn. 6 are known. Let $V_j(x, y)$ be the given potential on the resonators, $\tilde{P}_k^s(i)$ in eqn. 6 are known. Let $V_j(x, y)$ be the given potential at the $j$th resonator and $j \leqslant N_r$, then $V(1) = \sum_{j=1}^{R} V_j(x, y)$ and $V(2) = \sum_{j=R+1}^{Nr} V_j(x, y)$. By setting $V_j(x, y) = 1$ at the $j$th resonator and keeping the other resonators on ground potential, the matrix eqn. 5 is solved to obtain the unknown coefficients $a_j^t$, $j = 1, 2, \ldots, N_r$, $t = 1, 2, \ldots, T_j$. Next, the charge distributions on the resonators can be computed from eqn. 4 by solving the unknown coefficient $a_j^t$. Then, the $j$th column vector of the capacitance matrix $[C_{ij}]$ associated with an $N_r$-resonator system is obtained by the following expression derived in a similar way, parallel to what is shown in Reference 18. By repeating the previous processes for $j = 1$–$N_r$, a square $N_r \times N_r$ capacitance matrix is then obtained.

$$\frac{1}{C_{ij}} = \frac{\oint \rho_j(x, y)v_j(x, y)\,dx\,dy}{\oint \rho_i(x, y)\,dx\,dy \oint \rho_j(x, y)\,dx\,dy} \quad (7)$$

The stationary property [18, 19] for $C_{ij}$ in eqn. 7 does not guarantee the charge distribution $\rho_j(x, y)$ at the $j$th resonator is the nearly true charge distribution of the $N_r$-resonator system. Unless the nearly true charge distributions on the resonators are obtained, the element value $C_{ij}$ is still subject to error, even if the solution for $C_{ij}$ seems to converge. The clue for this problem is the use of correct basis functions in the SDA.

In the case of two-dimensional full-wave analyses of planar or quasi-planar transmission lines, it has already been shown that a set of basis functions is capable of representing nearly true current distributions for a variety of transmission lines [20, 21]. Here, however, we assume that only the quasi-TEM mode may propagate in the filter. Thus, the transverse current components are discarded, e.g. the second equation in eqn. 1 of Reference 20 or eqns. 10 and 11 of Reference 21. Left with the longitudinal current components and extending these longitudinal current components from the two-diemnsional problem to the three-dimensional problem, a new set of basis functions for our particular problem and its relation to the total charge distribution of a resonator will be described as follows: Consider, for example, the charge distribution $\rho_{i+1}$ on the resonator $R_{i+1}$ in Fig. 2*a*. By using the normalised variables $U = (x - x_{i+1})/(l_{i+1}/2)$ and $V = (y - y_{i+1})/(W/2)$, where $l_{i+1}$ and $W$ are the physical length and width of the resonator, respectively, the unknown charge distribution $\rho_{i+1}$ is expressed by

$$\rho_{i+1}(x, y) = \sum_{r=1}^{4}\sum_{p=1}^{P}\sum_{q=1}^{Q}a_{i+1}^{rpq} \times \xi^{rpq}(x, y) \quad |x - x_{i+1}| \leqslant (l_{i+1}/2) \quad |y - y_{i+1}| \leqslant (W/2) \quad (8)$$

where $P$ and $Q$ are positive integers and

$$\xi^{1pq}(x, y) = [(1 + U)^{p/2-1} - \sqrt{(2)}(1 + U)^{(p+1)/2-1} + 0.5(1 + U)^{(p+2)/2-1}] \times [(1 + V)^{q/2-1} - \sqrt{(2)}(1 + V)^{(q+1)/2-1} + 0.5(1 + V)^{(q+2)/2-1}] \quad (9a)$$

$$\xi^{2pq}(x, y) = [(1 - U)^{p/2-1} - \sqrt{(2)}(1 - U)^{(p+1)/2-1} + 0.5(1 - U)^{(p+2)/2-1}] \times [(1 + V)^{q/2-1} - \sqrt{(2)}(1 + V)^{(q+1)/2-1} + 0.5(1 + V)^{(q+2)/2-1}] \quad (9b)$$

$$\xi^{3pq}(x, y) = [(1 + U)^{p/2-1} - \sqrt{(2)}(1 + U)^{(p+1)/2-1} + 0.5(1 + U)^{(p+2)/2-1}] \times [(1 - V)^{q/2-1} - \sqrt{(2)}(1 - V)^{(q+1)/2-1} + 0.5(1 - V)^{(q+2)/2-1}] \quad (9c)$$

$$\xi^{4pq}(x, y) = [(1 - U)^{p/2-1} - \sqrt{(2)}(1 - U)^{(p+1)/2-1} + 0.5(1 - U)^{(p+2)/2-1}] \times [(1 - V)^{q/2-1} - \sqrt{(2)}(1 - V)^{(q+1)/2-1} + 0.5(1 - V)^{(q+2)/2-1}] \quad (9d)$$

The derivation of the basis functions for the two-dimensional problem has been documented in Reference 21. Only the physical significance, however, will be discussed here. As every resonator is rectangular in shape, the basis functions are individually expanded with respect to the four corner points on the assumed infinitely thin rectangular metal strip, as shown in eqns. 9*a–d*. The global basis function $\xi^{1pq}$ in eqn. 9*a*, for instance, is expanded at the bottom left corner point $(U, V) = (-1, -1)$, where the $\delta^{-1/2}$ singularity is satisfied by the first term, i.e. $p = q = 1$, at $(U, V) = (-1, -1)$. This $\delta^{-1/2}$ singularity is also guaranteed for the two edges intersecting at this corner point $(U, V) = (-1, -1)$. Furthermore, $\xi^{1pq}$ vanishes at the other three corner points $(U, V) = (1, -1)$, $(-1, 1)$ and $(1, 1)$ and the two edges connected by these three points for all positive integers $p$ and $q$. The higher-order nonsingular components, containing $(1 + U)^0$, $(1 + U)^{0.5}$, $(1 + U)^1$, ..., and $(1 + V)^0$, $(1 + V)^{0.5}$, $(1 + V)^1$, ..., are also included in eqn. 9*a* for $p > 1$ and $q > 1$. Eqns. 9*b–d* are derived in the same way as eqn. 9*a*. As a result, eqns. 9*a–d* are independent of each other and they all satisfy the edge condition imposed on the assumed infinitely thin metal strip. Replacing eqn. 4 by eqn. 8 and substituting the Fourier transform of $\xi^{rpq}$, $r = 1, 2. 3, 4$ into eqns. 5*a*, 5*b* and 6, a linear matrix equation is obtained for solving the unknown coefficients $a_j^{rpq}$, $j = 1, 2, \ldots, N_r$, $r = 1, 2, 3, 4$, $p = 1, 2, \ldots, P$, $q = 1, 2, \ldots, Q$. Finally, the charge distribution $\rho_{i+1}(x, y)$ on the resonator $R_{i+1}$ is the superposition of $a_{i+1}^{rpq} \times \xi^{rpq}(x, y)$ shown in eqn. 8.

### 2.2 De-embedding procedure for the discontinuity parameters

To de-embed the gap-coupled discontinuity parameters ($jB_{si}$ and $jB_{pi}$) shown in Fig. 2*b*, we first obtain the $2 \times 2$ capacitance matrix associated with two adjacent gap-coupled resonators $R_i$, $R_{i+1}$ by invoking the three-dimensional quasi-TEM SDA described in Section 2.1. The symmetric $2 \times 2$ capacitance matrix representation of the two gap-coupled resonators consists of the following constituent components: The first is the total bulk capacitance of the uniform SSS. The second is the SSS open-end fringing field capacitance at one end of the resonator. The third is the susceptances of the equivalent $\pi$-network at the gap-coupled discontinuity. The discontinuity parameters are simply contributed by the last (third) components. Therefore we need to remove the capacitances contributed by the first two components.

The line capacitance $C_0$(F/m) of the SSS is obtained by the two-dimensional quasi TEM SDA [14] having the same cross-sectional geometry as the three-dimensional one. The open-end fringing field capacitance $C_e(F)$ is obtained by analysing a single resonator using the three-dimensional quasi-TEM SDA. Following the procedure described by Itoh *et al.* [17], $C_e$ is given by

$$C_e = \tfrac{1}{2}[C_r - l \times C_0] \quad (10)$$

where $C_r$ is the total capacitance of the single resonator, and $l$ is the length of the resonator. In the calculation, $l$ is a finitely large value beyond which the change of $C_e$ is negligible. Note that $C_e$ is not variational, although the expression for $C_r$ given in eqn. 7 is stationary.

Now we can de-embed the discontinuity parameters between the two adjacent gap-coupled resonators. $C_{12}$ of the $2 \times 2$ capacitance matrix represents the series coupling between the two resonators. Therefore

$$B_{si}/\omega = -C_{12} \quad (11)$$

Note that $C_{12}$ is negative in value. $(C_{11} + C_{12})$ is the total capacitance of the resonators $R_i$ with respect to ground. Then, the remaining discontinuity parameter $B_{pi}$ can be expressed as

$$B_{pi}/\omega = (C_{11} + C_{12}) - l_i \times C_0 - C_e \quad (12)$$

As $C_{12}$ is variational, $B_{si}$ is variational too. $B_{pi}$, however, is no longer variational. Thus, how to obtain the nearly true charge distributions of the two gap-coupled resonators is an important issue, which has already been discussed in Section 2.1.

### 2.3 Validity check

Before obtaining the discontinuity parameters for designing the gap-coupled SSS bandpass filter, the accuracy of the de-embedding approach described so far has to be verified. This can be established by two steps. The first one will answer the question of how many basis terms are required to have a converged solution for the capacitance matrix. The second is that the results obtained by our approach should agree with the available data, which are obtained both experimentally the theoretically.

Fig. 3 plots the total capacitance of a long rectangular microstrip resonator against $P$, which is the number of basis functions in $x(U)$ direction expanded at one of the four corners of the resonator. The physical parameters of such a resonator are also given in Fig. 3. When using the spectral terms of $M = N = 5000$ and increasing the value of $P$ from 2 to 6 with the value of $Q$ as a controlling parameter, Fig. 3 indicates that the condition when $P = Q = 3$ will result in a good converged value for the total capacitance of the resonator.

Using eqn. 10 under the conditions $M = N = 5000$ and $P = Q = 3$, Fig. 4 plots the open-end effect ($2\,\Delta l$) against microstrip width ($W$). The calculated results based on our de-embedding process are shown by the solid line, which coincides with the asterisk data points obtained by the resonance measurements [22] performed between 11.33 GHz and 12.26 GHz. The open-end effect data extracted from the full-wave SDA resonance technique at 12 GHz [22] are shown by the dotted line. The three-dimensional quasi-TEM de-embedding approach,

using the new set of basis functions, shows very good agreement between the computed and measured results for the microstrip open-end effect.

By setting $\psi_i = 0°$, $t_i = 0.0$ mm and $v_i = 0.0$ mm in our formulation, the discontinuity parameter associated with

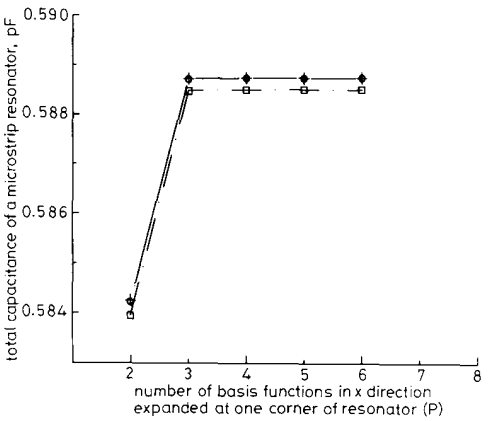


**Fig. 3** *Convergence of the total capacitance of a long rectangular microstrip resonator by the three-dimensional quasi-TEM SDA*

$a = 20$ mm; $b = 20$ mm; $h_1 = h_2 = 0.3$ mm; $h_3 = 10.0$ mm; $\varepsilon_1 = \varepsilon_2 = 9.47$; $\varepsilon_3 = 1.0$; $W = 0.3$ mm; $l = 4.5$ mm. The central point of the microstrip resonator projected in the $x$-$y$ plane is located at (10 mm, 10 mm)

□···□ $Q = 2$
○···○ $Q = 3$
+—+ $Q = 4$
$M : N = 5000 : 5000$

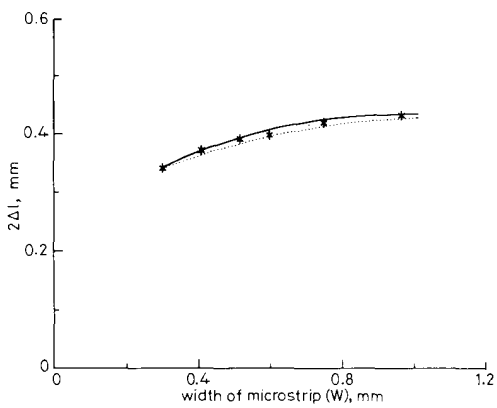


**Fig. 4** *Microstrip open-end effect* ($2\Delta l$) *against the width of microstrip resonator* ($W$)

Associated structural parameters are $a = 20$ mm; $b = 20$ mm; $h_1 = h_2 = 0.3$ mm; $h_3 = 10.0$ mm; $\varepsilon_1 = \varepsilon_2 = 9.47$; $\varepsilon_3 = 1.0$; and $l = 4.5$ mm. The central point of the microstrip resonator projected in the $x$-$y$ plane is located at (10 mm, 10 mm). The calculated results by the three-dimensional quasi-TEM SDA are under condition $P = Q = 3$ and $M = N = 5000$

——— Results calculated by three-dimensional quasi-TEM SDA
* * * Measured results [21]
- - - - Results calculated at 12 GHz by three-dimensional full-wave SDA resonance method [21]

two colinear end-coupled SSS resonators can be obtained. Prior to the computation of the discontinuity parameters, a similar convergence study was performed. The results showed that $P = 6$ and $Q = 3$ will be sufficient to have all the element values in the $2 \times 2$ capacitance matrix converge to less than 0.05%. In Fig. 5, the values for the equivalent $\pi$-circuit elements $B_{si}/\omega$ and $B_{pi}/\omega$ against the gap spacing ($u_i$) between the adjacent resonators are plotted. The solid lines obtained by our approach are in excellent agreement with the data extracted from Fig. 3 of Reference 23, using the rigorous three-dimensional spectral-domain hybrid mode approach developed by Jansen.

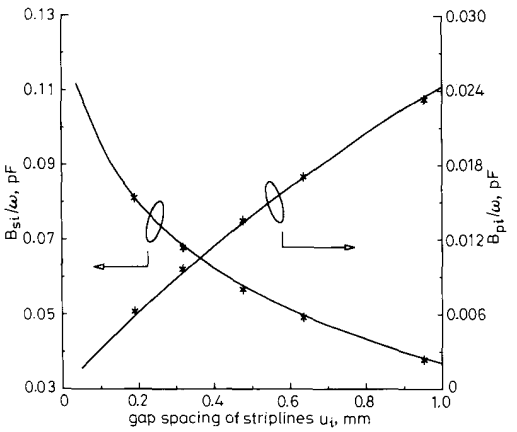


**Fig. 5** *Equivalent circuit elements* $B_{si}/\omega$ *and* $B_{pi}/\omega$ *of the end-coupled SSSs against the gap spacing* $u_i$

Associated structural parameters are $a = 30$ mm; $b = 6.985$ mm; $h_1 = h_2 = 0.635$ mm; $h_3 = 6.35$ mm; $\varepsilon_1 = \varepsilon_3 = 1.0$; $\varepsilon_2 = 10.4$; $t_i = 0.0$ mm; $\psi_i = 0°$; $v_i = 0.0$ mm; $l_i = l_{i+1} = 5.0$ mm; and $W = 0.635$ mm. The calculated results obtained by our approach are under $P = 6$, $Q = 3$ and $M = 5000$, $N = 1000$

* * * Results extracted by full-wave, three-dimensional SDA (frequency = 4 GHz) [22]
——— Results calculated by authors' approach

### 2.4 Discontinuity parameters for use in the experimental filter synthesis

The validity check established in the Section 2.3 allows us to design the gapcoupled filter illustrated in Fig. 1. This section will describe the filter design procedure for an experimental prototype, which incorporates both 90°-bent gap-coupled resonators, assuming $\psi_i = 90°$, $t_i = 0.254$ mm, and the colinear end-coupled resonators, assuming $\psi_i = 0°$, $t_i = 0.0$ mm (see Fig. 2*a*). This implies that our prototype will have certain adjacent resonators placed perpendicular to each other. The 0.254 mm thick RT-5880 Duroid substrate of $\varepsilon_r = 2.2$ is used. Fig. 6 plots the $\pi$-circuit discontinuity parameters of the 90°-bent gap-coupled (colinear end-coupled) resonators, under solid (broken) lines, against the gap discontinuity parameter $u_i$, where $v_i$ is assumed to be $u_i$ or $-u_i(0.0$ mm). When $u_i$ is smaller than one-half resonator width ($W/2$), the adjacent 90°-bent gap-coupled reonators overlap each other, and the overlapping region is square in shape. When $u_i$ is greater than $W/2$, there is no overlapping region defined. Instead, the shortest distance of two adjacent resonators projected into the $x$-$y$ plane is $\sqrt{(2)}(u_i - W/2)$. When the coupling between the resonators is strong, or $u_i < 0.34$ mm for the case of 90°-bent gap-coupled resonators, the parallel susceptance $B_{pi}$ becomes inductive. The change-over phenomenon was also observed and reported by Jansen [23] for the asymmetric series gap-coupled microstrips and SSSs. Note that, prior to obtaining the data shown in the solid line, the convergence study must be performed. The results showed that the least number of terms for $P$ and $Q$ is six to have the converged solution for the capacitance matrix in the present case study. The data shown in both solid

and broken lines will be further used by the filter synthesis equations described in the following section to establish two look-up tables for designing an experimental filter.

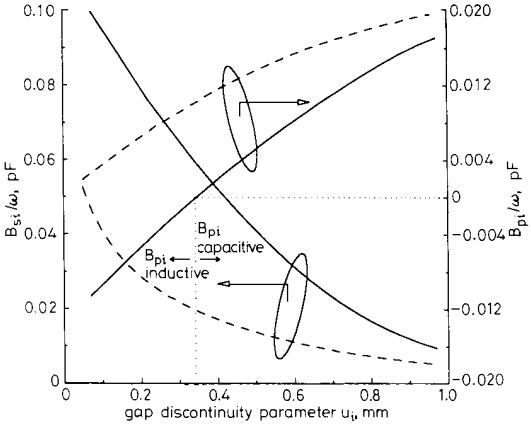


**Fig. 6** *Series circuit elements ($B_{si}/\omega$) and parallel circuit elements ($B_{pi}/\omega$) of the equivalent π-circuit of the gap-coupled discontinuities as functions of the gap discontinuity parameter $u_i$*

Structural parameters are $a = 30$ mm; $b = 30$ mm; $h_1 = h_3 = 0.6$ mm; $h_2 = 0.254$ mm; $\varepsilon_1 = \varepsilon_3 = 1.0$; $\varepsilon_2 = 2.2$; $l_1 = l_2 = 5.0$ mm; and $W = 1.84$ mm. The calculated results are obtained under $M = N = 5000$, and $P = 6$, $Q = 6$ for the 90°-bent gap-coupled discontinuity, $P = 6$, $Q = 3$ for the colinear end-coupled resonators

- - - - Colinear end-coupled discontinuity ($t_i = 0$, $u_i = 0$, $\phi_i = 0$)

——— 90°-bent gap-coupled discontinuity ($t_i = 0.254$ mm, $v_i = u_i$ or $u_i$, $\phi_i = 90°$)

## 3 Design for an experimental K-band gap-coupled bandpass filter

### 3.1 Filter synthesis equations using admittance inverter [16]

As the experimental filter prototype to be developed is a bandpass filter with less than 20% fractional bandwidth, the filter synthesis based on admittance inverters [16] will provide sufficient accuracy for the specified filter characteristics. For the sake of clarity, the following outlines the filter synthesis procedure already reported in Reference 16. The filter synthesis begins with the following expressions:

$$\frac{\omega'}{\omega_1'} = \frac{1}{W}\left(\frac{\omega}{\omega_0} - \frac{\omega_0}{\omega}\right) \tag{13}$$

$$\omega_0 = \sqrt{(\omega_1 \times \omega_2)} \tag{14}$$

$$W = \frac{\omega_2 - \omega_1}{\omega_0} \tag{15}$$

where $\omega$ and $\omega'$ represent the angular frequencies in the bandpass and the lowpass domains, respectively, and $\omega_0$, $\omega_1$ and $\omega_2$ are the given midband, lower and upper cutoff angular frequencies of the bandpass filter, respectively. $\omega_1^*$ is the cutoff angular frequency of the lowpass prototype, and $w$ is the fractional bandwidth of the bandpass filter. Given the bandpass filter response of $\varepsilon$ dB, equal ripple in the passband and the filter degree of $n$, the corresponding normalised elements' values $g_i$, $i = 1, 2, \ldots, n$, of the lowpass prototype can be obtained either by the use of Table 4.05–2 or eqn. 4.05–2 in Reference 16. Knowing the normalised elements' values, the admittance inverters with parameters $J_{i,i+1}/Y_0$, $i = 0, 1, \ldots, n$, are given by

$$J_{0,1}/Y_0 = \sqrt{[\pi w/(2g_0 g_1 \omega_1')]} \tag{16a}$$

$$J_{i,i+1}/Y_0 = \pi w/[2\omega_1'\sqrt{(g_i g_{i+1})}] \tag{16b}$$

$$J_{n,n+1}/Y_0 = \sqrt{[\pi w/(2g_n g_{n+1} \omega_1')]} \tag{16c}$$

where $g_0$ and $g_{n+1}$ are the generator and load impedances of the lowpass prototype, respectively. $Y_0$ is the normalised admittance of the bandpass filter. Once the above parameters of the admittance inverters are determined, one can design the physical layout for the prototype filter using the discontinuity parameters reported in Section 2.4. The ideal admittance inverter is approximated by the equivalent π-circuit of the gap-coupled discontinuities in series with two transmission lines with electrical length $\Phi_{i,i+1}$, as shown in Figs. 7. Applying the following two exprs. 17 and 18, based on the data shown in Fig. 6, two look-up tables are generated and shown in

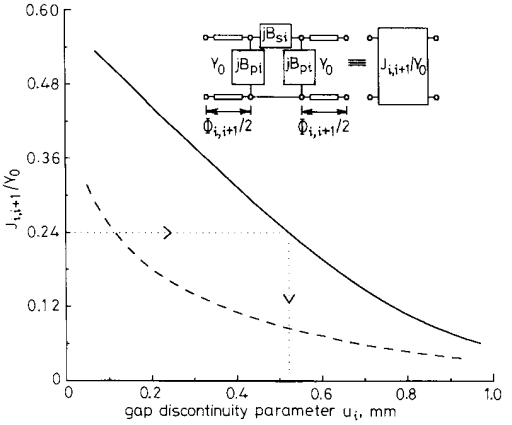


**Fig. 7A** *Admittance inverter parameter $J_{i,j+1}/Y_0$ corresponding to the coupling structures of Fig. 6 against the gap discontinuity parameter $u_i$*

- - - - Colinear end-coupled discontinuity ($t_i = 0$, $v_i = 0$, $\phi_i = 0$)

——— 90°-bent gap-coupled discontinuity ($t_i = 0.254$ mm, $u_i = u_i$ or $-u_i$, $\phi_i = 90°$)

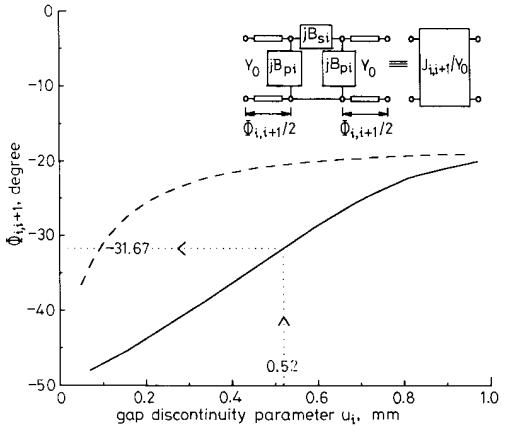


**Fig. 7B** *Electrical line length $\Phi_{i,j+1}$ (see eqn. 18) corresponding to the coupling structures of Fig. 6 against the gap discontinuity parameter $u_i$*

- - - - Colinear end-coupled discontinuity ($t_i = 0$, $v_i = 0$, $\phi_i = 0$)

——— 90°-bent gap-coupled discontinuity ($t_i = 0.254$ mm, $u_i = u_i$ or $-u_i$, $\phi_i = 90°$)

Figs. 7A and B for the admittance parameters $J_{i,i+1}/Y_0$ and the electrical line length $\Phi_{i,i+1}$, respectively.

$$J_{i,i+1}/Y_0 = |\tan [\Phi_{i,i+1}/2 + \tan^{-1}(B_{pi}/Y_0)]| \quad (17)$$

$$\Phi_{i,i+1} = -\tan^{-1}(2B_{si}/Y_0 + B_{pi}/Y_0) - \tan^{-1}(B_{pi}/Y_0) \quad (18)$$

where $B_{si}$ and $B_{pi}$ are evaluated at midband frequency $f_0 = 21.494$ GHz, and $Y_0$ is normalised at 0.02. The value of $\Phi_{i,i+1}$ computed from eqn. 18 is negative for most gap-coupled discontinuities. These negative electrical lengths $\Phi_{i-1,i}$ and $\Phi_{i,i+1}$ are absorbed into the $i$th half-wavelength SSS resonator. The electrical length of this resonator becomes

$$\theta_i = 180^\circ + (\Phi_{i-1,i} + \Phi_{i,i+1})/2 \quad (19)$$

The use of the look-up tables illustrated by Figs. 7A and B will be explained by the following filter prototype design example.

### 3.2 Experimental bandpass filter design

Fig. 8 shows the circuit layout of the experimental bandpass prototype employing both 90°-bent gap-coupled resonators and colinear end-coupled resonators.

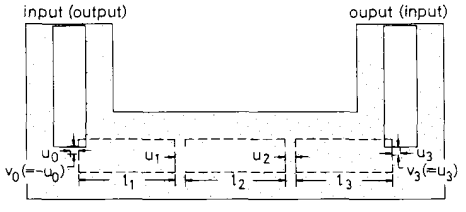


**Fig. 8** *Circuit layout of experimental three-resonator gap-coupled SSS bandpass filter*

Resonators with solid lines are on the top surface of the substrate, and those with broken lines are on the bottom side of the substrate. The gap discontinuity parameters $u_i$, $i = 0, 1, 2, 3$ and the physical length of the resonators $l_i$, $i = 1, 2, 3$, will be determined by the use of Figs. 7A and B

Such an implementation, using various types of coupling structure, results in the input and output ports being located at the same reference plane, which in turn results in zero compressed length for the filter. The 90°-bent gap-coupled discontinuities are at both the lower left and the lower right corners of the circuit layout, where the input and output ports are connected to the top SSSs, shown in solid lines. The first, second and third resonators are underneath the substrate and are perpendicular to the input and output SSSs. The first (second) and second (third) resonators are arranged in the colinear end-coupled fashion.

Given the specifications that assume 0.2 dB equal ripple passband loss between 21 and 22 GHz and the filter degree of three, as already implied in Fig. 8, one may obtain the parameter values of the admittance inverter by using eqns. 16*a–c*. Once those values have been obtained, the gap discontinuity parameters $u_i$, $i = 0, 1, 2, 3$ and the physical length of the resonators $l_i$, $i = 1, 2, 3$, as shown in Fig. 8, are determined by the use of Figs. 7A and B. For example, starting with the admittance inverter parameter of 0.24 for the 90°-bent gap-coupled resonators, one can follow the arrow symbols shown in Fig. 7A to determine the value of the gap discontinuity parameter $u_0$ (or $u_3$). Starting from this value $u_0(u_3)$, which is 0.52 mm in this particular case, one can follow the arrow symbols again to determine the value of $\Phi_{i,i+1}$ in Fig. 7B. Once all the values of $\Phi_{i,i+1}$ for $i = 0, 1, 2, 3$ are obtained, the electrical length of the three resonators are determined by eqn. 19. Therefore the design is completed by knowing all the gap discontinuity parameter $u_i$, $i = 0, 1, 2, 3$ and the electrical length $\theta_i$, $i = 1, 2, 3$.

## 4 Comparison between theoretic and experimental results

Fig. 9 is a photograph of the experimental filter together with the structural parameters corresponding to Fig. 2*a* and Fig. 8. The SSS resonators on the 0.254 mm thick RT–5880 Duroid substrate are placed symmetrically in a 1.454 mm high and 4 mm wide rectangular waveguide housing. All the resonators have the same 50 Ω characteristic impedance. It is found that, under these design parameters, the SSS has the cutoff frequency of the first higher-order mode at about 36 GHz [21], which is far beyond our stopband frequency of interest in our prototype design.

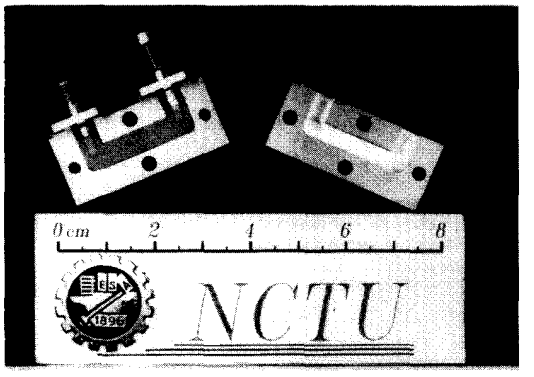


**Fig. 9** *Photograph of a 21–22 GHz three-resonator gap-coupled SSS bandpass filter prototype placed in a 1.454 mm high and 4 mm wide rectangular waveguide housing*

Structural parameters corresponding to Fig. 2A and Fig. 8 are $h_1 = h_3 = 0.6$ mm; $h_2 = 0.254$ mm; $\varepsilon_1 = \varepsilon_3 = 1.0$; $\varepsilon_2 = 2.2$; $W = 1.84$ mm; $l_1 = l_3 = 5.52$ mm; $l_2 = 5.73$ mm; $t_0 = t_3 = 0.254$ mm; $\psi_0 = \psi_3 = 90°$; $u_0 = u_3 = 0.52$ mm; $v_0 = -0.52$ mm; $v_3 = 0.52$ mm; $t_1 = t_2 = 0.0$ mm; $\psi_1 = \psi_2 = 0°$; $u_1 = u_2 = 0.65$ mm; $v_1 = v_2 = 0.0$ mm

Fig. 10 superimposes the plots for the measured filter responses and the theoretic predictions for the insertion loss and the return loss of a zero compressed length, 21–22 GHz three-resonator gap-coupled bandpass filter prototype, respectively. The theoretic results are obtained by the Touchstone™ microwave circuit simulation, provided with the discontinuity parameters $B_{si}/\omega$ and $B_{pi}/\omega$, $i = 0, 1, 2, 3$ and the complex propagation constants accounting for the lossy SSSs with various physical lengths $l_i$, $i = 1, 2, 3$. The complex propagation constant $(\alpha + j\beta)$ for the SSS at 21.494 GHz was found to be $\beta = 1.0846k_0$ and $\alpha = 5.57 \times 10^{-3}$ dB/mm, based on the rigorous full-wave mode-matching program [24] assuming 10 μm thick copper strip with conductivity $\sigma = 5.85 \times 10^7$ (S/m). The measured filter responses show less than 1.4 dB insertion loss and greater than 10 dB return loss in the passband.

The filter was constructed by a typical hybrid microwave integrated circuit (MIC) photolithography process which has 0.02 mm resolution tolerance. Neither tuning nor layout compensation of any kind was conducted. In

Fig. 10, both measured and theoretic filter responses are in excellent agreement. This also confirms the accuracy of our de-embedding procedure for the gap-coupled discontinuities described in Section 2.

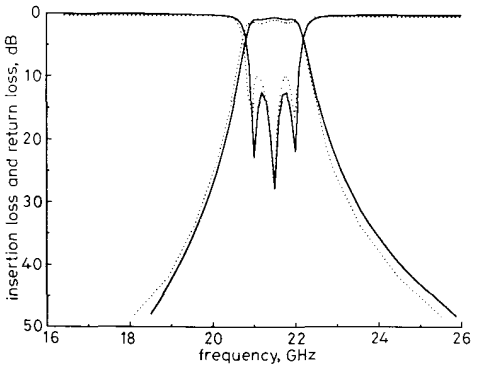


**Fig. 10** *Theoretic and measured filter responses of a 21–22 GHz three-resonator gap-coupled SSS bandpass filter prototype*

——— Theoretic filter responses
····· Measured filter responses

## 5 Conclusions

A new gap-coupled SSS bandpass filter design is presented in detail. The new filter configuration can orient the resonators in any arbitrary direction. This makes the new filter highly flexible to interface with other microwave circuit components and eliminates all possible forms of interference among them.

The fact that the SSS gap-coupled resonators are very complicated in shape and possess no symmetry mandates an accurate and efficient de-embedding algorithm to determine the equivalent $\pi$-circuit parameters of the gap-coupled discontinuity problem for carrying out the filter synthesis. A de-embedding procedure described in Section 2, employing the three-dimensional quasi-TEM SDA incorporating a new set of basis functions, was validated by the data existing in the literature.

The design procedure described, which involves two look-up tables, enables the physical layout of the gap-coupled filter to be determined very quickly, although the filter is complicated in shape. A 21–22 GHz zero compressed length bandpass filter, consisting of both 90°-bent gap-coupled resonators and colinear end-coupled resonators, was built and tested. Both measured and predicted filter responses agree very well in both passband and stopband. The constructed filter is the first-pass design requiring neither tuning nor adjustment. Thus, the filter design technique presented here is proved to be suitable for the MIC process, which makes it cost-effective and reproducible.

## 6 References


1 RHODES, J.D.: 'Suspended substrate filters and multiplexers'. Proceedings of 1986 European Microwave Conference, 16th EuMc, pp. 8–18
2 DEAN, J.E.: 'Suspended substrate stripline filters for ESM applications', *IEE Proc. F, Commun., Radar & Signal Process*, 1985, **132,** (4), pp. 257–266
3 DEAN, J.E.: 'Microwave integrated circuit broadband filters and continguous multiplexers'. PhD thesis, University of Leeds, 1979
4 MOBBS, C.I., and RHODES, J.D.: 'A generalized Chebyshev suspended substrate stripline bandpass filter', *IEEE Trans.*, 1983, **MTT-31,** (5), pp. 397–402
5 LÖSCH, I.E., and MALHERBE, J.A.G.: 'Design procedure for inhomogeneous coupled line sections', *IEEE Trans.*, 1988, **MTT-36,** (7), pp. 1186–1190
6 LEVY, R.: 'New equivalent circuits for inhomogeneous coupled lines with synthesis applications', *IEEE Trans.*, 1988, **MTT-36,** (6), pp. 1087–1094
7 RUBIN, D., and HISLOP, A.R.: 'Millimeter-wave coupled line filters', *Microw. J.*, 1980, **23,** pp. 67–78
8 TON, T.N., SHIH, Y.C., and BUI, L.Q.: '18–30 GHz broadband bandpass harmonic reject filter'. Digest of 1987 IEEE MTT-S *International Microwave Symposium*, Session J–37, pp. 387–389
9 NGUYEN, C., and CHANG, K.: 'Design and performance of millimeter-wave end-coupled bandpass filters', *Int. J. Infrared & Millim. Waves*, 1985, **6,** (7), pp. 497–509
10 DOUGHERTY, R.M.: 'MM-wave filter design with suspended stripline', *Microw. J.* 1986, **29,** pp. 75–84
11 TZUANG, C.-K.C., CHIANG, Y-C., and SU, S.: 'Design of a quasi-planar broadside end-coupled bandpass filter'. Digest of 1990 IEEE MTT-S *International Microwave Symposium*, Session I–36, pp. 407–410
12 ZYSMAN, G.I., and JOHNSON, A.K.: 'Coupled transmission line networks in an inhomogeneous dielectric medium', *IEEE Trans.*, 1969, **MTT-17,** (10), pp. 753–759
13 RHODES, J.D.: 'Design formulas for stepped impedance distributed and digital wave maximally flat and Chebyshev low-pass prototype filters', *IEEE Trans.*, 1975, **CAS-22,** (11), pp. 866–874
14 ITOH, T.: 'Generalized spectral domain method for multiconductor printed lines and its application to turnable suspended microstrips', *IEEE Trans.*, 1978, **MTT-26,** (12), pp. 983–987
15 NAGHED, M., and WOLFF, I.: 'Equivalent capacitances of coplanar waveguide discontinuities and interdigitated capacitors using a three-dimensional finite difference method', *IEEE Trans.*, 1990, **MTT-38,** (12), pp. 1808–1815
16 MATTHAEI, G.L., YOUNG, L., and JONES, E.M.T.: 'Microwave filters, impedance-matching networks, and coupling structures' (McGraw Hill, New York, 1964), Chaps. 8 and 4
17 ITOH, T., MITTRA, R., and WARD, R.D.: 'A method for computing edge capacitance of finite and semi-infinite microstrip lines', *IEEE Trans.*, 1972, **MTT-20,** (12), pp. 847–849
18 COLLIN, R.E.: 'Field theory of guided waves' (The Institute of Electrical and Electronics Engineers, Inc., New York 1991), p. 278
19 JANSEN, R.H.: 'The spectral-domain approach for microwave integrated circuits' *IEEE Trans.*, 1985, **MTT-33,** (10), pp. 1043–1056
20 TZUANG, C.-K.C., and KUO, J.-T.: 'Modal current distribution on closely coupled microstrip lines: a comparative study of the SDA basis functions', *Electron. Lett.*, 1990, **26,** (7), pp. 464–465
21 KUO, J.-T., and TZUANG, C.-K.C.: 'Complex modes in shielded suspended coupled microstrip lines', *IEEE Trans.*, 1990, **MTT-38,** (9), pp. 1278–1286
22 UWANO, T.: 'Accurate characterization of microstrip resonator open end with new current expression in spectral-domain approach', *IEEE Trans.*, 1989, **MTT-37,** (3), pp. 630–633
23 KOSTER, N.H.L., and JANSEN, R.H.: 'The equivalent circuit of the asymmetrical series gap in microstrip and suspended substrate lines', *IEEE Trans.*, 1982, **MTT-30,** (8), pp. 1273–1279
24 TZUANG, C.-K. C., CHEN, C.-D., and PENG, S.-T.: 'Full-wave analysis of lossy quasi-planar transmission line incorporating the metal modes', *IEEE Trans.*, 1990, **MTT-38,** (12), pp. 1792–1799